14. Geochemical Characteristics

By W. Ian Ridley

14 of 21

Volcanogenic Massive Sulfide Occurrence Model

Scientific Investigations Report 2010–5070–C

U.S. Department of the Interior
U.S. Geological Survey

U.S. Department of the Interior
KEN SALAZAR, Secretary

U.S. Geological Survey
Marcia K. McNutt, Director

U.S. Geological Survey, Reston, Virginia: 2012

Suggested citation:
Ridley, W. Ian, 2012, Geochemical characteristics in volcanogenic massive sulfide occurrence model: U.S. Geological Survey Scientific Investigations Report 2010–5070 –C, chap. 14, 18 p.

Contents

Figures

Tables

14. Geochemical Characteristics

By W. Ian Ridley

Trace Elements and Element Associations

Volcanogenic massive sulfide deposits are important resources of base and precious metals and a variety of rare elements. The precious and rare metals usually are present at trace concentrations, but natural refining of such metals can determine the economic viability of a deposit. The list of trace elements includes the following: Co, Ni, Ga, Ge, As, Se, Mo, Ag, Cd, In, Sn, Sb, W, Au, Hg, Tl, and Bi. The proportions of metals and their concentrations are largely a function of the overall rock associations and fluid chemistry. For instance, in Canadian VMS deposits, felsic-dominated deposits have high Pb and Ag, whereas the bimodal-felsic deposits contain the highest Au concentrations. In many cases, the trace-element associations are determined by the overall chemistry of the various lithologies that are encountered by fluid during hydrothermal circulation, and they may be determined by lithologies that are distal to the deposit. For instance, the Mount Read deposits in Tasmania carry anomalously high concentrations of Au that appear to have been sourced from distal high-Ti basalts (Stolz and Large, 1992). Volcanogenic massive sulfide deposits, associated primarily with mafic and ultramafic assemblages, tend to have high Co, Ni, and Se concentrations (Galley and others, 2007).

Trace elements may precipitate during mixing of reduced hydrothermal fluids with heated or ambient seawater as a function of the sulfidation state of the fluid. Modern and ancient VMS deposits cover a wide range of sulfidation states based on sulfide mineral assemblages and associated alteration assemblages (Sillitoe and others, 1996). In the presence of low to intermediate sulfidation minerals (pyrrhotite, pyrite, chalcopyrite, arsenopyrite, tennantite, high-Fe sphalerite, galena), trace metals may precipitate as native elements (Bi, Ag, Hg, Sb, Sn). These conditions appear to be mostly met in Cu-Zn deposits associated with mafic assemblages and minor felsic components. In the presence of intermediate to very high sulfidation minerals (pyrite, bornite, digenite, enargite, low-Fe sphalerite), trace elements tend to be fixed in sulfides and sulfosalts, such as famantinite (Cu_3SbS_4), cinnabar (HgS), berthierite ($FeSb_2S_4$), bismuthinite (Bi_2S_3), stibnite (Sb_2S_3), argentite (Ag_2S), and tennantite ($[Cu,Fe]_{12}As_4S_{13}$) but may also be associated with native Au. In active marine hydrothermal systems, high sulfidation fluids are associated with island-arc settings, and in ancient VMS deposits they occur in siliciclastic-felsic and felsic lithologic associations (Sillitoe and others, 1996). A list of deposits with high sulfidation characteristics is shown in table 14–1. In many cases, the precipitation of exotic minerals that represent only trace constituents is paragenetically late and spatially associated with barite-rich lithologies, consistent with an increase in sulfidation state with decreasing temperature. The close spatial association with advanced argillic and alunitic alteration indicates that the hydrothermal fluids were highly acidic and corrosive, and the high sulfidation state of the fluids may indicate the involvement of magmatic fluids and gases. This also may be the source of some of the trace elements associated with the high sulfidation minerals.

Zoning Patterns

All VMS deposits show some degree of geochemical/mineralogical zoning that is a function of fluid composition, fluid mixing, temperature, and porosity/permeability. In ancient VMS deposits, the geochemical/mineralogical evolution of deposit growth is difficult to follow, as the later stages of sulfide precipitation tend to overprint earlier stages and there commonly have been several stages of ore mineralization. However, studies of modern black smoker chimneys, for example, those at 21°N and 9°50'N on the East Pacific Rise and at the TAG active hydrothermal field at the Mid-Atlantic Ridge, provide insights into the evolution of sulfide growth. To some degree, these patterns are microcosms of the larger scale zonation observed at the deposit scale because in both cases the mineralogic zonation is a function of fluid chemistry (mixing between hydrothermal fluid and seawater) and a steep temperature gradient (hydrothermal fluid at up to 400 °C and ambient seawater at 1–2 °C). In modern chimney growth, the critical initial stage is the precipitation of anhydrite [$CaSO_4$] ± caminite [$Mg_7(SO_4)_5(OH)_4 \cdot H_2O$] from conductively heated seawater as a consequence of the reverse solubility of these minerals. It is the outward and upward precipitation of anhydrite at the seawater interface that stabilizes chimney growth and provides a matrix for precipitation of sulfide phases (Haymon, 1983). The chimney advances upward and outward by anhydrite growth. Hot hydrothermal fluid that circulates

Table 14–1. Modern and ancient volcanogenic massive sulfide deposits with high sulfidation state minerals (after Sillitoe and others, 1996).

[Ag, silver; As, arsenic; Au, gold; Bi, bismuth; Cu, copper; Zn, zinc; al, alunite; and, andalusite; aspy, arsenopyrite; ba, barite; bn, bornite; cass, cassiterite; cc, chalcocite; cinn, cinnabar; cor, corumdum; cord, cordierite; cp, chalcopyrite; cv, covellite; dia, diaspore; dig, digenite; en, enargite; gal, galena; gyp, gypsum; id, idiate; kao, kaolinite; ky, kyanite; luz, luzonite; marc, marcasite; mont, montmorillonite; musc, muscovite; ns, native sulfur; po, pyrrhotite; py, pyrite; pyro, pyrophyllite; qz, quartz; rut, rutile; ser, sericite; sp, sphalerite; sulf, sulfosalts; tenn, tennantite; tetra, tetrahedrite; top, topaz; zir, zircon; Mt, million metric tons; g/t, gram per ton]

Name	Grade, tonnage	Age	Host rocks	Minealization style	Hypogene alteration	Hypogene sulfides
Hine Hina, Lau Basin	no data	Recent	Andesites	Seafloor massive sulfide	qz, kao,pyro, al, ns, ba	sp, py, marc, bn, cp, tenn, gal, sulf
Undu, Fiji	1.5×105 t 6% Cu, 7% Zn	Pliocene	Dacitic pumice breciia	Massive sulfide pods in pipelike body	qz, kao, mont, gyp, ba	py, cp, sp, gal, en, tenn, cv, id
Tsuchihata, Japan	>4.5 Mt 1.2% Cu, Au + Ag	Miocene	Rhyolite dome	Stockwork	qz	py, cp, tetra, en, luz
Kizilkaya, Turkey	10 Mt 1% Cu, 1.5% Zn	Cretaceous	Dacitic volcanics	Stockwork and massive sulfide remnants	qz, ser, kao, dia	py, sp, cp
Brewer, USA	4.6 Mt 14 g/t Au	Late Proterozoic–Early Cambrian	Volcanics and volcanoclastics	Pipe breccia, massive sulfides	and, cord, pyro, al, top, ba, dia, rut, zir	py, en, cv, bn, tenn, cass, Bi, sp, gal, cinn
Boliden, Sweden	8.3 Mt 1.4% Cu, 6.8% As, 15 g/t Au, 50 g/t Ag	Proterozoic	Dacite, qz porphyry, schist	Pipelike massive sulfide	qz, and, musc, dia, cor	py, cp, aspy, po, sp, gal, sulf
Bousquet, Canada	No. 1: 20.7 Mt 4.5 g/t Au; No. 2: 7.4 Mt 6.1g/t Au, 16 g/t Ag, 0.6% Cu	Archean	Qz-sericite schist	Stockwork and massive sulfide	qz, and, ky, musc	py, bn, cp, sp, cc, dig, tenn

within the anhydrite matrix close to the seawater interface is rapidly cooled and precipitates fine-grained, metastable pyrrhotite (po) and Fe-rich sphalerite (sp). As the anhydrite-sulfide matrix grows outward, the inner wall pyrrhotite is replaced by stable pyrite (py) as a result of the admixture of hydrothermal fluid and seawater. Pyrite becomes the dominant mineral phase during chimney growth. Once the chimney structure is established by anhydrite growth, the hydrothermal fluid is isolated and high temperature phases precipitate. Pyrite + Cu-Fe sulfides (chalcopyrite (cp), cubanite (cb; $CuFe_2S_3$)) precipitate at the inner wall so that the chimney grows inward (fig. 14–1) and also outward, replacing the anhydrite matrix. The diameter of the inner fluid-filled channel is maintained at an equilibrium value as a function of the fluid flow rate, which determines the rate of sulfide precipitation and the rate of abrasion of precipitated material.

Haymon (1983) recognized four different pathways of further chimney evolution: one bornite (bn) sequence and three bornite-absent sequences (a chalcopyrite-dominant sequence, a chalcopyrite-intermediate solid solution (iss) sequence, and a cubanite sequence). These four sequences represent a gradual change in mineralogy (largely by replacement), pS_2, Eh, pH, fluid mixing, and temperature, from an early bornite mineralogy to a late cubanite mineralogy.

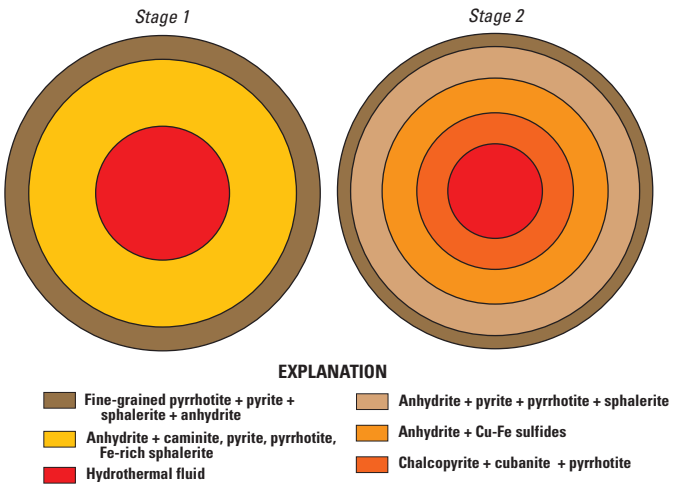

Figure 14–1. Idealized cross sections through the two main stages of growth of a massive sulfide chimney. Stage 1 involves initial deposition of anhydrite followed by precipitation of Fe sulfides and Fe-rich sphalerite in the porous network of anhydrite minerals. The chimney grows outward by addition of anhydrite to the outer chimney wall due to heating of ambient seawater by hot hydrothermal solutions diffusing outward from the central fluid core. Stage 2 growth involves deposition of high-temperature sulfides (chalcopyrite, isocubanite, pyrrhotite) from hydrothermal fluids that are essentially shielded from contact with cool seawater. Percolation of hydrothermal fluid across the chimney wall results in cooling and precipitation of lower temperature sulfides, such as sphalerite. Modified from Haymon (1983). [Cu, copper; Fe, iron]

The bornite sequence involves the precipitation of a sheath of cp around the central fluid channel, followed outward by a zone of bn(Cu_5FeS_4) + chalcocite (cc; Cu_2S) and a zone of covellite (cv; CuS)+ digenite (dg; Cu_9S_5)+ anhydrite, all of which are accompanied by precipitation of py + sp. This is a sequence of outwardly increasing Cu/Fe ratio, sulfidation, and oxidation state. The chalcopyrite-dominant sequence has a central sheath of cp with outward increase in Cu/Fe ratio and an outer sheath of randomly distributed cp + iss + cp-iss + cb + py + sp in an anhydrite matrix. In the cp-iss sequence, the inner sheath of cp with outward increase in Cu/Fe ratio is surrounded by a sheath of cp-iss + iss with an outward decrease in Cu/Fe ratio. The cb series has a central sheath of cb (no cp) and an outer sheath of randomly scattered grains of cb + py + sp in an anhydrite matrix. The latter sequence forms in mature chimneys where hot (350 °C or hotter) fluids are sufficiently reduced to stabilize cubanite and pyrrhotite, which are also the common sulfide minerals observed in black smoker effluent quenched from 360 °C by ambient seawater.

A field of black (and white) smoker chimneys is not, of itself, an economic resource. In addition, the simple accumulation of black smoker debris on the seafloor would not mimic the clear geochemical/mineralogical zonation commonly observed in ancient VMS deposits. It would instead represent a spatially random collection of sulfide minerals. In 1985, a critical unknown link to ancient VMS deposits was solved with the discovery of the TAG active mound at the Mid-Atlantic Ridge, a roughly circular structure with an estimated total massive sulfide resource of 2.7 Mt (2 percent Cu) and 1.2 Mt of mineralized stockwork breccia (1 percent Cu). The TAG mound was subsequently drilled during Leg 158 of the Ocean Drilling Project, thus providing a three-dimensional perspective of the development of a modern VMS deposit (fig. 14–2). Although the open ocean setting of the TAG deposit probably has no equivalent in ancient VMS deposits, it does have chemical, mineralogical, and volcanological similarities to Cyprus-type VMS deposits.

Probably the most important discovery at TAG was the recognition of intermittent periods of fluid flow within and beneath the sulfide mound, interspersed with periods of fluid discharge at the mound surface. The intermittent behavior was assumed to be in response to: (1) periods of enhanced porosity/permeability within the mound due to mineral dissolution and hydro-fracturing that allowed for dispersed fluid flow at low flow rates and limited entrainment of seawater, and (2) periods of porosity/permeability occlusion due to mineral precipitation (mainly anhydrite, due to the conductive heating of small volumes of seawater) that led to focused, high-rate fluid flow with enhanced entrainment of seawater. The movement of fluid from the base of the deposit (including the underlying stockwork zone) toward the deposit/seawater interface has produced a zone refining effect. The zone refining results from the interplay of variable temperature and fluid chemistry. The periodic movement of high temperature fluids preferentially incorporates phases precipitated earlier from lower temperature fluids. For instance, the preferential dissolution

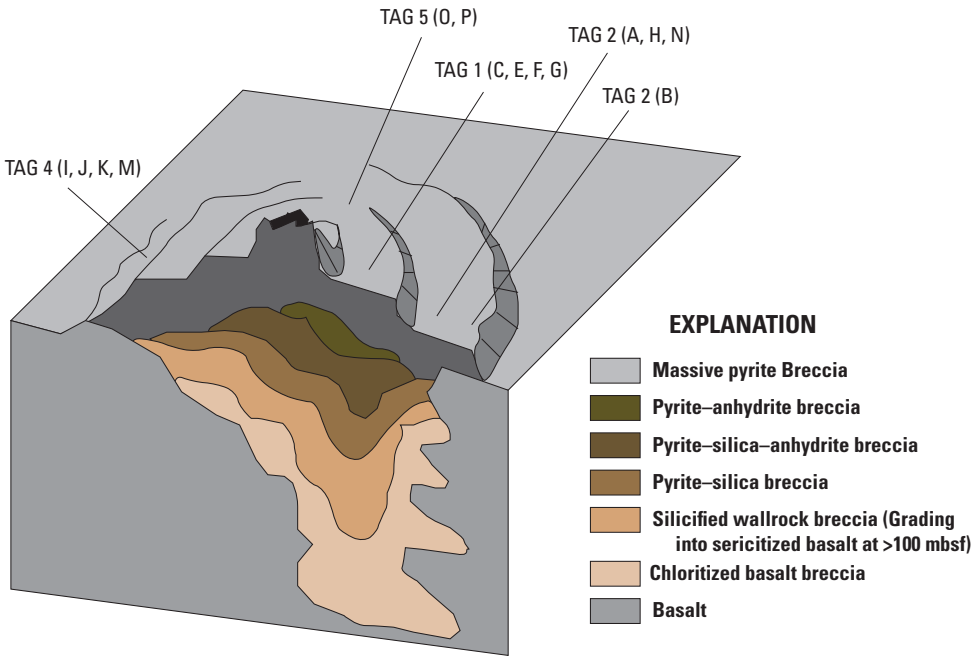

Figure 14–2. Idealized cross section through the Trans-Atlantic Geothermal (TAG) hydrothermal field based on Alvin dive observations and Ocean Drilling Program (ODP) drilling during Leg 158. The ODP holes are shown at TAG 1–5. The TAG field is a combination of inactive vents and active black smoker vents, a mound of sulfide breccia and a carapace of iron oxides (ochres) and weathered sulfide. Drilling has revealed a mineralogically and chemically zoned deposit lying above a silicified stockwork. The main sulfide body is composed of a complex assemblage of sulfide-anhydrite-quartz breccia, but containing very low base metal concentrations compared to surface samples. This is due to continuous zone-refining that causes dissolution of low-temperature minerals and redeposition at the seawater interface. Modified from Humphris and Tivey (2000) and Petersen and others (2000). [mbsf, meters below sea floor]

of Zn-S phases results in the zone purification of Cu-Fe-S ore. The periodic movement of fluids that are undersaturated with respect to some previously precipitated phases also results in dissolution and mass transfer along the fluid gradient. The overall effect is the preferential movement of major and trace elements along a thermal gradient that results in purification, but it also results in the concentration of trace elements into economic grades at the low temperature part of the zone refining pathway. For instance, at the TAG mound, dissolution and recrystallization has produced an almost pure Cu-Fe-S deposit leached of Zn, Cd, Ag, Sb, Pb, and Au that are now redeposited and concentrated within the upper 10 m of the deposit. In principle, the end result would be a barren pyritic ore and the loss and dispersal of other base and other metals into the water column through zone refining, secondary supergene enrichment, and seafloor weathering.

Zone refining provides a useful model for the zonal patterns observed in ancient VMS deposits (Galley and others, 2007). In back-arc mafic settings, the stockwork is frequently a subsurface breccia of chlorite + pyrite and quartz + pyrite beneath a core of massive pyrite and pyrite + quartz breccia. The latter is sheathed with a marginal facies of sphalerite + chalcopyrite covered with a banded jasper-chert carapace. In the bimodal mafic-felsic setting, the stockwork frequently shows a complex zoned mineralogy that grades outward from pyrrhotite + pyrite + chalcopyrite through quartz + chlorite and chlorite + sulfide to sercite + chlorite. The main sulfide ores grade outward from massive pyrite + pyrrhotite + chalcopyrite to massive pyrite + sphalerite + chalcopyrite. In the bimodal felsic setting, the massive ore commonly grades outward from chalcopyrite + pyrrhotite + pyrite through pyrite + sphalerite + chalcopyrite, pyrite + sphalerite + galena to pyrite + sphalerite + galena + tetrahedrite + Ag + Au. In the felsic-siliciclastic setting, the stockwork zone is highly siliceous and associated with chlorite + pyrrhotite + pyrite + chalcopyrite and may also be Au-bearing, as observed at several of the Mount Read deposits. The massive ores are commonly pyrite + pyrrhotite + chalcopyrite with some Au mineralization grading outward to layered pyrite + sphalerite + galena + Au + Ag.

Thus, zone refining provides an efficient way for upgrading the base metal and precious metal grades of VMS deposits (Shwarz-Schampera and Herzig, 2002). In settings dominated by felsic volcanics, the base metal association of Fe-Zn-Pb-Cu dominates and these deposits frequently contain high-graded, economic amounts of Au, Ag, Sn, Sb, Bi, Co, and In, such as in deposits found at Kidd Creek. Such deposits commonly have a Cu-rich base and a Zn ± Pb carapace. In addition, there exists a temperature-dependent element fractionation. First, a high-temperature suite forms involving the limited solubility of Cu, Co, Se, In ± Ni. Second, a low-temperature suite forms, determined by a combination of solubility and volatility, involving Zn, Ag, Au, Pb, Hg, Cd, Bi, Sn, Sb, As, Ga, Hg, ± Tl ± W. These high-graded metals may be present as complex sulfides, such as roquesite (CuInS), amalgams, selenides, and sulfosalts.

Fluid-Inclusion Thermometry and Geochemistry

Unlike modern VMS systems where hydrothermal fluids can be sampled directly, no such luxury applies in ancient VMS systems where the chemistry of hydrothermal (and metamorphic) fluids can only be sampled in fluid inclusions. Minuscule volumes of trapped fluids occur in a variety of gangue and ore minerals, but in most cases, studies are limited to inclusions encased in either gangue quartz or low-Fe sphalerite ore. Fluid inclusions most frequently have been used to measure temperatures of entrapment and fluid salinity utilizing microthermometry and, in rare cases, attempts have been made to directly measure gas content (CO_2, CH_4, N_2, SO_2, H_2S), major cation concentrations (Na, K, Ca, Mg), trace cation concentrations (ore elements: Fe, Cu, Zn, Pb, Ba; gangue elements: B, Li, Sr, Rb), and major anions (Cl, S, Br). The several techniques that are used in the study of fluid inclusions have been discussed in detail by Shepherd and Rankin (1998) and Brown (1998).

Fluid inclusions provide an opportunity to understand various aspects of ore deposition processes, including variations in temperature and salinity as a function of ore deposition evolution, fluid mixing and phase separation, and sources of fluids (and hence sources of metals and anions). Table 14–2 illustrates the wide variety of hydrothermal fluid temperatures and salinities observed in gangue and ore minerals involved in the formation of VMS deposits. Most studies of fluid inclusions in VMS deposits have recognized salinities close to seawater values and enhanced salinities in fluids that are generally interpreted as modified seawater. In the latter case, salinity may be increased during hydration reactions with rock minerals along the hydrothermal fluid pathways. In some cases, very high salinities are encountered that may be interpreted as the result of fluid boiling to produce a brine and low-salinity vapor, phase separation at depth, a magmatic fluid, or fluid interactions with evaporates. The fluid salinity is important because it largely determines fluid density, which in turn determines if the hydrothermal fluid acts as a buoyant liquid when mixed with seawater and cooled or lacks buoyancy and ponds at the seafloor/seawater interface. In the case of buoyant hydrothermal plumes (as observed in modern black and white smoker systems), probably >95 percent of the entrained metals are lost from the immediate site of venting. In the case of stagnant hydrothermal fluids, probably >95 percent of the metals are retained at the site of fluid venting.

A number of studies of the siliciclastic-felsic associated deposits of the Iberian Pyrite Belt deposits have been carried out. These include studies at Neves Corvo and Salgadinho in Portugal and Tharsis, Concepción, San Miguel, Aguas Teñidas, San Telmo, Rio Tinto, and Aznalcóllar in Spain. At Aznalcóllar, the fluids increase in temperature and salinity with depth and toward the central, highly altered stockwork across a range of 200–400 °C. In addition, a low temperature, low salinity fluid also has been trapped that can be interpreted as either cooling upon mixing with a meteoric fluid or the presence of a cooled condensed vapor phase subsequent to fluid boiling (Almodovar and others, 1998). At Rio Tinto, high temperature fluid inclusions have not been found; the majority lies within a narrow temperature range of 130–230 °C with salinities between 2 and 10 percent NaCl equivalent (Nehlig and others, 1998). Evidence for postmineralization redistribution of metals has been found in metamorphic fluids trapped in inclusions at the Tharsis deposits (Marignac and others, 2003) and the Salgadinho deposit (Inverno and others, 2000). The former study is particularly interesting in demonstrating that metamorphic fluids peaked in temperature at 430 °C at 300 MPa pressure and then dropped to 170 °C at 40 MPa, a difference that the authors attributed to a change from lithostatic to hydrostatic conditions.

A detailed fluid inclusion study was carried out by Hou and others (2001) on the Gacun bimodal-felsic deposit in Sichuan, China. They demonstrated an increase in temperature and salinity with depth within the stringer zone involving very high salinity fluids (17–21 percent NaCl equivalent) of unknown origin. Overall, the fluid salinities varied from 4 to 21 percent, the lower values associated with late-stage, low-temperature barites.

There have been surprisingly few fluid inclusion studies of the siliciclastic-felsic associated VMS deposits of Japan, the major contribution being Pisutha-Arnond and Ohmoto (1983). In the Hokuroku District, they demonstrated variations in temperature from 200 to 380 °C but very small variations in fluid salinity (3–6 percent NaCl equivalent). The greatest temperature range was observed in the black ore minerals (200–330 °C), whereas the yellow ore minerals had a limited range (330±50 °C).

At the siliciclastic-felsic Hellyer deposit, Tasmania, Zaw and others (1996) identified three phases of vein development associated with mineralization. Fluid inclusion from these three phases (2A, 2B, 2C) and a postmineralization vein system provided both temperature and salinity information. Phase 2A inclusions in quartz and sphalerite

Table 14–2. Fluid inclusion thermometry and chemical compositions for selected volcanogenic massive sulfide deposits.

[Ca, calcium; Cl, chlorine; Cu, copper; Fe, iron; K, potassium; Mg, magnesium; Mn, manganese; Na, sodium; Pb, lead; Zn, zinc; TH, temperature; °C, degree Celcius; mmol, millimols; ppm, parts per million; eq, equivalents; temp, temperature; ass., associated]

Deposit	Mineral	TH °C	Salinity NaCl equivalent	Na mmol	K mmol	Ca mmol	Mg mmol	Mn mmol
Hokuroku District, Japan								
Uwamuki 2	Chalcopyrite	200–400		220–310	9–38			
	Quartz	200–500		76	7		6	
Uchinotai West	Pyrite	200–400		280–470				
	Quartz	300–500						
Fukazawa	Pyrite	200–400		63–720	48–130	47–100	1–14	
	Sphalerite	200–400		260–380	56		8	
Furutobe	Sphalerite	200–400		410			5	
Matsumine	Quartz	200–500		75–120	27–37	37–48	13	
Shakanai	Pyrite	200–400		390	26			
	Quartz	200–500		150–730	3–50	3–30	2	
Gacun, China								
	Barite	99–125	2.1–13.2					
	Sphalerite	125–221	6.1–14.5					
	Quartz	150–310	4.2–10.4					
	Barite	196–217	6.4–9.3					
	Sphalerite	213–258	5.7–12.9					
	Quartz	150–350	6–20.5					
	Sphalerite	185–260	5.1–7.8					
	Quartz	299–319	17.1–21.3					
	Barite	208–357	5.9–16.8					
Iberian Pyrite Belt, Spain and Portugal								
Rio Tinto	Quartz	109–330	2–10					
Salgadinho	Quartz	225–235	4.2–5.7					
Aznalcollar	Quartz	139–214	0.4–7.2					
	Quartz	203–299	1.2–8.3					
	Quartz	306–384	4.3–12.4					
Neves Corvo	Quartz	230–260	2–8	0.008–0.019*				
		280–370	~30					
Tharsis	Quartz	170–430	5.2–9.5					
Northern Iberian Pyrite Belt	?	130–280	6–14					
	?	82–110	16–24					
	Quartz	120–270	~4					
Matagami, Quebec								
Bell Allard	Quartz	212±34	15.8±4.7					
Isle Dieu	Quartz	191±18	17.7±4.9					
Orchan West	Quartz	178±10	18.2±2.7					
Mattagami Lake	Quartz	233±9	15.5±3					
Bell River Complex	Quartz	373±44	38.2±1.9					
Eskay Creek, British Columbia								
	Quartz	109–210		471–1,741**	43–3,360**			
	Sphalerite	96–200		537–2,650**	231–3,829**			
Hellyer, Tamania								
	Quartz	170–220	6.6–14.8		1,030–11,900#	913–10,300#		92–1,320#
	Quartz	165–322			2,910–43,900#	992–8,700#		140–493#
	Quartz	190–256						
	Quartz				1,280–1,220#	473–1,920#		94–335#

Table 14–2. Fluid inclusion thermometry and chemical compositions for selected volcanogenic massive sulfide deposits.—Continued

[Ca, calcium; Cl, chlorine; Cu, copper; Fe, iron; K, potassium; Mg, magnesium; Mn, manganese; Na, sodium; Pb, lead; Zn, zinc; TH, temperature; °C, degree Celcius; mmol, millimols; ppm, parts per million; eq, equivalents; temp, temperature; ass., associated]

Deposit	Cl mmol	SO_4 mmol	CO_2 mmol	CH_4 mmol	Cu ppm	Pb ppm	Zn ppm	Fe ppm
Hokuroku District, Japan								
Uwamuki 2	130–430		10–140					
	73							
Uchinotai West	5–480		350					
			240					
Fukazawa	22–270		210					
	20–580	150						
Furutobe	460							
Matsumine	290	130	60–250					
Shakanai	88							
	92–750	40–210	310		0–4.4	0–25	0–2.1	0–5.6
Gacun, China								
Iberian Pyrite Belt, Spain and Portugal								
Rio Tinto								
Salgadinho								
Aznalcollar								
Neves Corvo	0.008–0.019*		20–96*	3–80*				
Tharsis			3–25*	0.02–1				
Northern Iberian Pyrite Belt								
Matagami, Quebec								
Bell Allard								
Isle Dieu								
Orchan West								
Mattagami Lake								
Bell River Complex								
Eskay Creek, British Columbia								
	565–1,839**		0.02–0.99*	0.07–1.39*				
	700–1,780**		0.1–2.64*	0.35–1.17*				
Hellyer, Tamania								
	9,070–99,800#				153–170		105–889	235–13,300
	2,910–43,900#				237–12,800		373–6,660	858–27,200
	2,670–63,300#				61		99–286	50–591

Table 14–2. Fluid inclusion thermometry and chemical compositions for selected volcanogenic massive sulfide deposits.—Continued

[Ca, calcium; Cl, chlorine; Cu, copper; Fe, iron; K, potassium; Mg, magnesium; Mn, manganese; Na, sodium; Pb, lead; Zn, zinc; TH, temperature; °C, degree Celcius; mmol, millimols; ppm, parts per million; eq, equivalents; temp, temperature; ass., associated]

Deposit	Total salts wt. %	K/Na	Ca/Na	Mg/Na	Na/Cl	Comments	Reference
Hokuroku District, Japan							
						Black ore minerals TH = 200–300°C	
Uwamuki 2	1.3–2.1	0.04–0.12			0.72–1.7	Yellow ore minerals TH = 330±50°C	Pisutha-Arnond and Ohmoto (1983)
		0.08		0.08	3.3	Little change in salinity: 3.5–6 % NaCl eq	
Uchinotai West	2.7				1.0		
Fukazawa	1.4–5.2	0.08–0.18	0.12–0.14	0.004–0.03	0.85–11		
	1.5–2.6	0.15		0.03	0.65–2.6		
Furutobe	2.4			0.01	0.90		
Matsumine	1.0	0.31	0.15–0.31	0.02	1.2		
Shakanai	2.5	0.07			4.5		
	0.9–4.6	0.02–0.07	0.02–0.06	0.01	1–1.6		
Gacun, China							
						Upper massive ore	Hou and others (2001)
						Upper massive ore	
						Upper massive ore	
						Middle stringer zone	
						Middle stringer zone	
						Middle stringer zone	
						Lower stringer zone	
						Lower stringer zone	
						Mound	
Iberian Pyrite Belt, Spain and Portugal							
Rio Tinto						90% of inclusion have TH=130–230°C	Nehlig and others (1998)
Salgadinho							Inverno and others (2000)
Aznalcollar						High-T inclusions associated with central stockwork	Almodovar and others (1998)
						Temp and salinity increase with depth	
						Temp and salinity increase toward stockwork	
Neves Corvo						Low salinity, low T fluids are most common	Moura (2005)
						High T, high salinity fluids rare	
Tharsis						Fluids are from metamorphic overprint	Marignac and others (2003)
Northern Iberian Pyrite Belt						Most inclusions in this range	Sanchez-Espana and others (2000)
						Minor population due to local boiling and cooling	
						Regional metamorphic fluids	
Matagami, Quebec							
							Ioannou and others (2007)
Bell Allard						Low T fluids at all deposits carried Zn but low Cu	
Isle Dieu							
Orchan West							
Mattagami Lake							
Bell River Complex						Fluid in zone of hydrothermal cracking, original T = 650–670°C	
Eskay Creek, British Columbia							
						Most inclusions <140°C	Sherlock and others (1999)
						Most inclusions <150°C	
Hellyer, Tamania							
						Stage 2A quartz ass. with mineralization	Zaw and others (1996)
						Stage 2B quartz ass. with mineralization	
						Stage 2C quartz ass. with mineralization	
						Stage 4 quartz, post-mineralization metamorphic veins	

* mole %; ** mmol/L; # ppm

had homogenization temperatures of 170–220 °C, phase 2B inclusions were trapped at 165–320 °C, and phase 2C inclusions were trapped at 190–256 °C. The variations in salinity were relatively small (8–11 percent NaCl equivalent), and the temperature variations at each stage of vein formation were interpreted as reflecting the waxing and waning of a hydrothermal system.

In summary, fluid inclusions in gangue and ore minerals provide important information on the variability of fluid temperature and composition during periods of mineralization and on the involvement of meteoric waters and magmatic fluids. Often, the salinity data alone cannot be uniquely interpreted because involvement of magmatic fluids, boiling, mixing, and phase separation can all produce large variations in fluid salinity. More constrained interpretations are possible if fluid inclusion data are combined with other information, such as stable isotope composition of gangue minerals.

Stable Isotope Geochemistry

Recent reviews of traditional stable isotopes (δD, $\delta^{13}C$, $\delta^{18}O$, $\delta^{34}S$) are provided by Huston (1999) and Ohmoto (1986) for ancient VMS deposits and by Shanks (2001) for modern seafloor hydrothermal VMS systems. Reviews of nontraditional stable isotopes (B, Fe, Cu, Zn, Mo) are provided by Johnson and Bullen (2004), Beard and Johnson (2004), and Albarede (2004). In ore deposit studies, stable isotopes have been used to establish the sources of ore fluids (H, C, O, S), temperatures of ore deposition (S), and silicate alteration (O). In VMS deposits, stable isotopes also have been used to establish pathways of fluid movement (O), fluid origin (H, O, S), redox variations (C, S), and fluid phase separation (O, H). Nontraditional stable isotopes have been used to develop the overall isotopic variability in VMS deposits, to better understand the causes of isotopic fractionations, and to fingerprint sources of metals.

$\delta^{18}O$ and δD

In several studies of whole rock $\delta^{18}O$ in the footwall (stockwork) and some hanging-wall sections of VMS deposits, there is a systematic variation in $\delta^{18}O$ as a function of alteration intensity. The lowest $\delta^{18}O$ values are found where the silicate alteration is most intense, which usually corresponds to the central zone of sericitic alteration, for example, Fukazawa, Japan (Green and others, 1983), Hercules, Tasmania (Green and Taheri, 1992), and Feitais-Estacao, Portugal (Barriga and Kerrich, 1984). Where the deposits can be spatially associated with shallow, subvolcanic stocks, the region of low $\delta^{18}O$ values forms a carapace above the intrusion from which narrow zones of low- $\delta^{18}O$ alteration extend upward into stringer zones beneath individual deposits. In some cases, there is a progressive increase in $\delta^{18}O$ upwards through the subvolcanic sequence (Holk and others, 2008) that probably reflects the upward decrease in temperature from the magmatic heat source toward the surface. The low- $\delta^{18}O$ zones correspond to regions of focused high-temperature fluid flow surrounded by zones of higher $\delta^{18}O$ alteration that correspond to lower grade alteration mineralogies, such as montmorillonite and zeolite zones.

The final alteration $\delta^{18}O$ value is determined by a number of variables. Taylor (1977) and Green and others (1983) provide similar equations for integrating these variables (water/rock ratio, temperature of reaction, alteration mineralogy, initial bulk rock $\delta^{18}O$ value, fluid $\delta^{18}O$) into a single function. For VMS deposits, some of these variables can be measured or approximated. For instance, fluid $\delta^{18}O$ values have been measured in active seafloor hydrothermal systems (mean 0.91±0.37 per mil, 122 measurements; Shanks, 2001), in fluid inclusions in gangue quartz in ancient VMS deposits (-0.7±1.75 per mil), and in mineral pairs in which temperature is assumed. The fractionation of $\delta^{18}O$ between fluid and rock ($\Delta^{18}O_{R\text{-}W}$) as a function of temperature is approximated for felsic systems by using either the measured value for oligoclase-water, and for mafic systems by the measured value for bytownite-water, or by thermodynamic reaction path calculations. Given these constraints, Huston (1999) calculated altered rock $\delta^{18}O$ values as a function of water/rock (W/R) ratio and temperature. They showed that substantive negative changes in $\delta^{18}O$ relative to original fresh rock values (in this case, 8 per mil) can only be achieved at high W/R ratios and at high temperatures, whereas relative positive changes in $\delta^{18}O$ can only be achieved at high W/R ratios and low temperatures. This conclusion is fully consistent with the distribution of $\delta^{18}O$ in altered gangue assemblages described above. That is, hot hydrothermal fluids moving through silicate assemblages with high fracture porosity/permeability causes focused flow to produce alteration assemblages with low $\delta^{18}O$ values, whereas distal fluid flow at lower temperatures produces alteration assemblages with higher $\delta^{18}O$ values.

An important, but contentious, question concerns the origin of fluids for VMS deposits and, consequently, the origin of metals in VMS deposits (see Beaty and others, 1988, for a review). The stable isotopes of oxygen and hydrogen provide important, although somewhat ambiguous, information in this regard because the competing fluid sources (seawater and late-stage magmatic fluid) have quite different $\delta^{18}O$ and δD values (approx. 0 per mil for seawater $\delta^{18}O$ and δD, 5 to 10 per mil $\delta^{18}O$ and -35 to -50 per mil δD for magmatic fluids). Huston and Taylor (1999) and Taylor and Huston (1999) provide useful appraisals as to the shifts away from either seawater or magmatic fluid compositions of $\delta^{18}O$ and δD compositions in ore fluids. Some processes, such as evaporation and fluid/rock interactions, cannot reasonably produce the observed ore fluid isotopic variations, whereas mixing of magmatic fluid and seawater and (or) isoenthalpic boiling are both possible mechanisms.

$\delta^{34}S$

Useful reviews of sulfur isotope geochemistry in VMS deposits are given by Ohmoto (1986) and Huston (1999) and in modern seafloor massive sulfides by Shanks (2001). Given that sulfur is the major metalloid in VMS deposits, there are consequently many hundreds of sulfur isotope analyses available. The most comprehensive list is given by Huston (1999).

There is a significantly wider range of $\delta^{34}S$ in Phanerozoic sulfides compared to Archean and Proterozoic sulfides. Although the dichotomy is probably real, it also may reflect fewer determinations in Archean and Proterozoic deposits. Sangster (1968) was the first to recognize that the trend of $\delta^{34}S$ variation in Proterozoic and Phanerozoic VMS deposits closely paralleled the ancient seawater curve but was offset to lighter $\delta^{34}S$ values by about 18 per mil. Subsequent studies have confirmed the general notion that seawater sulfate provides a source of reduced sulfur for VMS deposits—a conclusion that is consistent with detailed studies of modern seafloor hydrothermal sulfide systems (Shanks, 2001; Rouxel and others, 2004a) in open ocean settings.

In modern island-arc and back-arc settings, $\delta^{34}S$ variability is more evident, with a greater proportion of vent fluids having light $\delta^{34}S$. The reasons for these shifts are not evident but may indicate a source of reduced sulfur in addition to seawater, such as a sulfur source from the disproportionation of magmatic sulfate ($SO_2 + 2H_2O \rightarrow H_2S + SO_4^{2-} + 2H^+$). In modern systems, the dominant role of seawater is also indicated by the $\delta^{34}S$ of anhydrite sulfate being almost identical to modern seawater sulfate. There are also other potential sources of reduced sulfur for Phanerozoic deposits, these being magmatic degassed H_2S (and possible SO_2) and sulfide leached from volcanic rock by circulating seawater. Because magmatic H_2S and sulfides in volcanics have overlapping values (0–5 per mil), it is not possible to directly differentiate between these two sources. Either source would act to offset seawater sulfide to lighter values. The reduction of seawater sulfate could occur through either abiotic or biotic processes. Abiotic processes involve redox reactions between sulfate and cations present in reduced form, (such as carbon, iron, and copper). Biotically-mediated reactions involve disproportionation reactions involving sulfate reducing bacteria (McCollom and Shock, 1997).

Most $\delta^{34}S$ studies involve either whole-rock determinations or analyses of mineral separates. However, the ability to now measure in situ relatively precise and accurate $\delta^{34}S$ values on single sulfide mineral grains demonstrates added complexity in interpreting sulfur isotope compositions of ancient VMS deposits. Slack and others (2008) analyzed pyrite, sphalerite, galena, chalcopyrite, and tetrahedrite from the Late Devonian–Early Mississippian Dry Creek deposit in east-central Alaska and demonstrated a range of $\delta^{34}S$ values from -48 to 23 per mil. They interpreted the isotopic data to reflect a two-stage mineralizing process. The first stage involved initial hydrothermal activity and mineralization in a local basin that was open to seawater sulfate. Sulfide $\delta^{34}S$ values reflected variable mixing of light anoxic pore fluid H_2S with oxic seawater sulfate to produce sulfides with $\delta^{34}S$ values between -40 and -10 per mil. Later sulfides formed in a Red Sea-type brine pool, producing $\delta^{34}S$ values of -10 to 9 per mil. Second, subsequent precipitation of sulfides (15–23 per mil) from anoxic bottom waters (10–60 per mil) formed when the basin became closed to oxic seawater. This type of highly detailed study is possible because the $\delta^{34}S$ data could be correlated both with mineral paragenesis and host lithology.

Unlike Phanerozoic deposits, VMS deposits of Proterozoic and Archean age have a much more limited range of $\delta^{34}S$ values, with a mean of about 0 per mil. If these data are truly representative, then different environmental conditions are implied. Although the seawater $\delta^{34}S$ curve cannot be extended into the Proterozoic and earlier (largely because of the lack of sulfate minerals associated with VMS deposits), the consistency of VMS $\delta^{34}S$ values (about 0 per mil) over 3 billion years of Earth history could only be achieved if: (a) the seawater sulfate value was close to the modern seawater value (approx. 21 per mil), and (b) ancient VMS deposits formed in the same way as Phanerozoic deposits. Both of these requirements may be correct, but there is no way to evaluate either criterion. Alternately, the geochemistry of Proterozoic and Archean oceans may have been fundamentally different because of a more anoxic atmosphere that limited the development of seawater sulfate (a layered ocean with only upper level sulfate) and limited the ocean bottom solubility of reduced sulfur under anoxic, alkaline conditions.

$\delta^{11}B$, $\delta^{64}Cu$, $\delta^{66}Zn$, $\delta^{57}Fe$, $\delta^{82}Se$

The first study of boron isotopes in modern VMS systems was by Spivack and Edmond (1987) for bare-ridge settings. They determined B concentrations and isotope values in vent fluids at 13°N and 21°N, concluding that boron was leached from basalts without resolvable fractionation and that such data can be used to fingerprint fluid/rock ratios and the global flux of B into the oceans. Other B isotope studies of vent fluids were carried out by James and others (1995) at Broken Spur and by Palmer (1996) at TAG and MARK (Mid-Atlantic Ridge at the Kane Fracture Zone) at the MAR and at the EPR. These studies demonstrated that the low-temperature removal of boron was a function of spreading rate.

Experimental studies by Spivack and others (1990) showed that B isotope systematics primarily reflected the proportions of B from seawater and crustal sources, and Seyfried and Shanks (2004) highlighted the usefulness of boron isotopes in constraining seafloor alteration and water/rock ratios.

The first B isotope study of ancient VMS deposits by Palmer and Slack (1989) reported data for tourmaline from 14 deposits of Archean to Ordovician age and showed a $\delta^{11}B$ value range from -15.7 to -1.5 per mil. They suggested six likely controls: (1) composition of the B source, (2) postore regional metamorphism (heavier, not lighter, isotope fractionates into the fluid phase, hence metamorphically recrystallized

tourmaline becomes isotopically lighter), (3) water/rock ratios, (4) seawater entrainment, (5) formational temperature, and (6) secular variations in seawater $\delta^{11}B$. The most important control was inferred to be the composition of the B source in footwall lithologies. Two topical studies have been reported for tourmaline associated with VMS deposits. Bandyopadhyay and others (1993) analyzed six tourmaline samples from small VMS deposits of Proterozoic age in India that showed a $\delta^{11}B$ range from -13.8 to -13.0 per mil, consistent with a B source dominantly from footwall pelitic schists and also possibly felsic volcanic rocks. Deb and others (1997) analyzed tourmaline from the large Deri VMS deposit in India (also Proterozoic) and reported $\delta^{11}B$ data for two tourmaline samples not from the ore zone of -16.4 and -15.5 per mil, which were interpreted to reflect leaching of felsic volcanic and argillaceous sedimentary rocks in the footwall sequence.

A detailed study by Taylor and Huston (1999) on 15 tourmalines in the feeder zone (mainly) and massive sulfide from the giant Kidd Creek deposit (Archean) reported $\delta^{11}B$ values from -13.6 to -7.8 per mil. Combined with data for O and H isotopes in the same tourmalines, they suggested that three fluids were involved in formation of the tourmalines (and by inference, the sulfides): (1) slightly modified seawater, (2) greatly modified seawater via previous subseafloor boiling, and (3) high-T supercritical fluid; the B isotope data in part imply fluid reaction with rocks that were previously altered at low temperatures.

Maréchel and others (1999) and Zhu and others (2000) first demonstrated the utility of transition metal isotopes as geochemical tracers. Transition metal isotopes have been applied to a variety of deposit types, including porphyry copper deposits (Larson and others, 2003; Graham and others, 2008; Markl and others, 2006; Mathur and others, 2009) and MVT (Mississippi Valley-type) deposits (Wilkinson and others, 2005), and have been examined experimentally (Ehrlich and others, 2004; Mathur and others, 2005). The application of nontraditional stable isotopes to VMS deposits is a relatively new enterprise that holds the promise of a deeper understanding of the source of metals to VMS systems and the various metal fractionations that might occur during the movement of hydrothermal fluids and the precipitation of sulfide minerals. In the environs of VMS deposits, the fractionation of transition metal isotopes is likely to be narrow at elevated temperatures and broader in situations that involve abiotic redox reactions and biotic reactions. Iron isotope behavior has been reviewed by Beard and others (2003), Beard and Johnson (2004), Johnson and others (2004); copper and zinc isotope behavior by Albarede (2004); and selenium isotopes by Johnson and Bullen (2004). Specific Fe isotope studies are found in Rouxel and others (2004a; 2008). Specific Cu isotope studies are found in Rouxel and others (2004b) and Mason and others (2005). Zinc isotope studies are found in Mason and others (2005), Wilkinson and others (2005) (MVT study) and John and others (2008). Table 14–3 shows ranges in transition metal isotopes that have been measured for modern and ancient VMS deposits.

Rouxel and others (2004a) have demonstrated that in modern hydrothermal sulfide systems both Fe and Se display mass-dependent fractionation. Se and S have very similar geochemistry. The usefulness of Se isotopes is that the Se/S ratio of seawater (6.3×10^{-8}) is very different than the mantle (MORB) values (1.5×10^{-4}), so that a combination of trace element analysis and isotopic determinations has the potential for recognizing different sources in hydrothermal systems. The Se isotopic composition ($\delta^{82}Se$) of modern seafloor hydrothermal sulfides varies by about 7 per mil and could result from a combination of redox reactions (selenate and selenide in seawater), biological reactions, and water/rock reactions. Rouxel and others (2002) indirectly measured the composition of modern seawater $\delta^{82}Se$ by assuming that the value was reflected in the isotopic composition of Mn-nodules (approx. -1.5 per mil). This value is thus indistinguishable from the mantle value so that the large variation of $\delta^{82}Se$ in sulfides could not be ascribed to mixing of volcanic Se with seawater Se. In addition, the Se/S ratio and Se concentration in seawater are so low that even partial reduction of oxidized forms of Se would have little effect on the $\delta^{82}Se$ of seafloor sulfides if seawater and hydrothermal fluid were mixed directly. However, redox reactions are the only known mechanism for producing very light Se, and there may be an unseen reservoir of light Se resulting from seawater redox reactions in the subsurface.

Rouxel and others (2004a) were the first investigators to take a multi-isotope (S-Se-Fe) approach to seafloor hydrothermal sulfide. The important contribution was the recognition of venting of pristine hydrothermal fluids that precipitated sulfides with Fe and Se isotopic values close to magmatic (about 0 per mil) accompanied by $\delta^{34}S$ values (approx. 1.5 per mil) that showed minimal involvement of seawater S. They also demonstrated other sulfide systematics that were consistent with substantial mixing of hydrothermal fluid and heated seawater and the necessity for a deep (subsurface) reservoir of light isotopic Se.

The $\delta^{57}Fe$ values of modern sulfide minerals appears to be a function of the environment in which the minerals either grew and (or) post-precipitation reworking, according to Rouxel and others (2008). These authors demonstrated a strong kinetic effect in the precipitation of iron sulfide minerals (pyrite, marcasite) during growth of active sulfide chimneys so that the $\delta^{57}Fe$ values were demonstrably different from vent fluid values. However, in inactive chimneys, the $\delta^{56}Fe$ values were essentially identical to vent fluid values, a result of postdepositional annealing.

There are relatively few studies of Cu and Zn isotopes in VMS deposits in modern and ancient settings. As a general conclusion, the isotopic fractionation of Zn ($\delta^{66}Zn$) is relatively small compared to copper ($\delta^{65}Cu$), largely as a reflection of its monovalent behavior. Mason and others (2005) report little variation in the $\delta^{65}Cu$ values of primary sulfides in the stockwork and massive sulfide zones of the Alexandrinka VMS deposit, but they report measurable differences in $\delta^{66}Zn$ variations between primary chalcopyrite and primary sphalerite, the former being lighter by about 0.4 per mil. They

Table 14–3. Some transitional metal isotope ratios in volcanogenic massive sulfide deposits and related rocks.

[Cu, copper; Fe, iron; Se, selenium; Zn, zinc; EPR, East Pacific Rise; MAR, Mid-Atlantic Ridge; ODP, Ocean Drilling Program; TAG, Trans-Atlantic Geothermal; U.S. Geological Survey geochemical reference materials: BCR, Basalt, Columbia River; BHVO, Basalt, Hawaiian Volcanic Observatory; BIR, Icelandic Basalt]

Deposit	Analysis type	δ64Cu per mil	δ66Zn per mil	δ57Fe per mil	δ82Se per mil	Comments	Reference
BCR-1 Standard	Whole rock			0.08 ± 0.1			
BIR-1 Standard	Whole rock			0.01			
BHVO-1 Standard	Whole rock			0.22 ± 0.13			
ODP Site 801C	Altered basalt			0.12 to 0.23		Fe isotope variations up to 4 per mil could be abiotic and (or) biotic	
	Deep-sea sediments			-0.07 to 0.23			
	Chemical sediments			-2.5 to 1.0			
	Chert			-2.5			
	Fe-oxyhydroxide sediments			-0.52 to 0.39			
	Celadonite			1.86			
Lucky Strike, MAR	Chalcopyrite	1.7 to 4.6, avg. 3.4		-0.12 ± 0.48	-3.22 ± 1.52	Variation in Cu isotopic composition due to sulfide oxidation	Rouxel and others (2004a, b)
	Atacamite	0.5 to 1.2, avg. 1.0					
	Pyrite/marcasite			-2.37 ± 0.46	-3.52 ± 1.15	Se-poor chalcopyrite has 57Fe -1 to -3 per mil. Se-rich chalcopyrite has 57Fe ~ 0 per mil. Abiotic fractionation of Fe isotopes during sulfide precipitation	
Logachev, MAR	Chalcopyrite	-1.0 to 0.7, avg. 0.14				Variation in isotopic composition due to sulfide oxidation	Rouxel and others (2004a, b)
	Atacamite	0.4 to 4.7, avg. 2.6					
	Bornite/covellite	-0.7 to 2.7, avg. 2.1				Variation in isotopic composition due to sulfide oxidation	

Table 14–3. Some transitional metal isotope ratios in volcanogenic massive sulfide deposits and related rocks.—Continued

[Cu, copper; Fe, iron; Se, selenium; Zn, zinc; EPR, East Pacific Rise; MAR, Mid-Atlantic Ridge; ODP, Ocean Drilling Program; TAG, Trans-Atlantic Geothermal; U.S. Geological Survey geochemical reference materials: BCR, Basalt, Columbia River; BHVO, Basalt, Hawaiian Volcanic Observatory; BIR, Icelandic Basalt]

Deposit	Analysis type	δ64Cu per mil	δ66Zn per mil	δ57Fe per mil	δ82Se per mil	Comments	Reference
Rainbow, MAR	Chalcopyrite/ isocubanite	0.11					Rouxel and others (2004a, b)
	Bornite/ covellite	3.3					
EPR 21oN	Vent fluids		0.31 ± 0.19			Fluid temperatures: 273–385oC	John and others (2008)
EPR 9oN	Vent fluids		0.56 ± 0.56	-0.54 ± 0.58		Fluid temperatures: 203–383oC	Rouxel and others (2008)
	Chalcopyrite		0.16 ± 0.07	-0.23 ± 0.09			
	Pyrite/ sphalerite/ galena		0.92 ± 0.28	-0.69 ± 0.02			
	Pyrite/sphal-erite		0.40 ± 0.42	-0.88 ± 0.34			
	Pyrite			-0.85 ± 0.50			
TAG, MAR	Vent fluids		0.25 ± 0.15			Fluid temperatures: 290–360oC	
Alexandrin-ka, Urals	Stockwork	0.12 to 0.30	0.45 to 0.05			Chalcopyrite, sphalerite, galena	Mason and others (2005)
	Main ore	0.28 to 0.32	-0.02 to 0.21			Sphalerite	

interpret this difference in terms of an equilibrium fractionation between the two phases, although this conclusion is at odds with the measurements made by John and others (2008) at modern hydrothermal sulfide settings. The observable differences in δ^{65}Cu values were associated with epigenetic versus supergene Cu phases, the latter being up to 0.6 per mil lighter as a result of isotopic fractionation associated with the reduction of Cu(II) to Cu(I) during supergene enrichment. Rouxel and others (2004a, b) observed δ^{65}Cu variations of up to 3 per mil in modern hydrothermal sulfide systems that they associated with seafloor oxidation of copper-bearing minerals. However, the δ^{65}Cu values became heavier in sulfides that had been subjected to seafloor weathering, and the isotopically heavy Cu was subsequently remobilized during further periods of high-T fluid flow and either redeposited at the periphery of the deposit or lost into the hydrothermal fluid.

Radiogenic Isotope Geochemistry

In base metal deposits, radiogenic isotopes are restricted to the study of lead isotopes in primarily galena and, more recently, rhenium-osmium (Re-Os) studies of a variety of sulfide phases. Reviews of Pb isotopes in a variety of ores, including a few VMS deposits, are provided by Gulson (1986) and Sangster and others (2000).

MVT and SEDEX deposits are the major global sources of Pb; there has been a proportionately large number of Pb isotope ratios measured for these two deposit types. VMS deposits do not constitute a major Pb source, and there is a limited literature dealing with their Pb isotopic signatures. However, Mortensen and others (2006) present an extensive compilation of lead isotopic compositions of sulfide samples from VMS deposits and occurrences in the northern North American Cordillera. Lead isotopes in galena, or other ore containing Pb and negligible U and Th, have the advantage that no age correction has to be made for the growth of radiogenic Pb. Consequently, the Pb isotopic composition reflects principally the age of the ore deposit (older deposits carry less radiogenic Pb) and secondarily the geochemistry (U/Th ratio) of the Pb source. Of the Pb isotope values for 151 deposits compiled by Sangster and others (2000), only 5 percent are for VMS deposits (Hellyer, Rosebery, Que River [Australia]; Verviers district [Belgium]; Bathurst district, Buchans, Buttle Lake [Canada]; Ambaji-Sendra belt [India]; Kuroko district [Japan]), of which only the Bathurst and Kuroko districts have been significant producers of Pb.

A new compilation of Pb isotope data that includes the previous compilation of Gulson (1986) for sulfides from a variety of VMS deposits is shown in table 14–4. Of particular note are the following: (1) the Pb isotope data for individual districts tend to be homogeneous, showing a maximum variation of about 2 percent; (2) the Pb isotope signature is the isotopic signature of the protolith, suggesting that either the individual protoliths are isotopically homogeneous or the hydrothermal systems are able to homogenize the Pb isotopic composition of heterogeneous protoliths; and (3) the Pb isotopic composition of ore galena has been used to define the lead crustal evolution (growth curves), so it follows that the calculated model ages should be close to the deposit ages.

Table 14–4. Lead (Pb) isotopic composition of selected volcanogenic massive sulfide deposits.

[Ba, barium; Cu, copper; Zn, zinc]

Deposit/district	Mineral	Age	$^{208}Pb/^{204}Pb$	$^{207}Pb/^{204}Pb$	$^{206}Pb/^{204}Pb$	Data source
			Tasmania, Australia			
Mount Read		Cambrian				
Rosebery-Hercules	Galena		38.064	15.598	18.271	Sangster and others (2000)
			38.083	15.609	18.273	
			38.081	15.606	18.272	
			38.041	15.594	18.266	
			38.068	15.603	18.279	
			38.041	15.594	18.273	
			38.053	15.583	18.277	
			38.053	15.595	18.272	
			38.138	15.611	18.286	
			38.093	15.608	18.276	
			38.047	15.597	18.268	
Que River	Galena		38.191	15.618	18.348	Sangster and others (2000)
			38.196	15.628	18.321	
			38.187	15.622	18.332	
			38.162	15.614	18.311	
			38.174	15.619	18.318	
			38.182	15.622	18.323	
			38.231	15.629	18.369	
			38.15	15.619	18.328	
			38.114	15.602	18.317	
			38.22	15.638	18.346	
			38.128	15.614	18.328	
			38.143	15.613	18.331	
			38.166	15.621	18.328	
			38.253	15.644	18.359	
			38.233	15.637	18.355	
Hellyer	Galena		38.219	15.624	18.372	Sangster and others (2000)

References Cited

Albarede, F., 2004, The stable isotope geochemistry of copper and zinc, *in* Johnson, C.M., Beard, B.L., and Albarede, F., eds., Geochemistry of non-traditional stable isotopes: Reviews in Mineralogy and Geochemistry, v.55, p. 409–427.

Almodovar, G.R., Saez, R., Pons, J.M., Maestre, A., Toscano, M., and Pascual, E., 1998, Geology and genesis of the Aznalcollar massive sulfide deposits, Iberian Pyrite Belt, Spain: Mineralium Deposita, v. 33, p.111–136.

Bandyopadhyay, B.K., Slack, J.R., Palmer, M.R., and Roy, A., 1993, Tourmalinites associated with stratabound massive sulfide deposits in Proterozoic Sakoli Group, Nagpur District, Central India, *in* Maurice, Y.T., ed., Eighth quadrennial IAGOD symposium, Ottawa, Canada, 12–18 August 1990, Proceedings: International Association on the Genesis of Ore Deposits, Stuttgart, Germany, E. Schweizerbart'sche Verlag, p. 867–885.

Barriga, F.J.A.S., and Kerrich, R., 1984, Extreme ^{18}O-enriched volcanics and ^{18}O-evolved marine water, Aljustrel, Iberian pyrite belt—Transition from high to low Rayleigh number convective regimes: Geochimica et Cosmochimca Acta, v. 48, p. 1021–1031.

Beard, B.L., and Johnson, C.M., 2004, Fe isotope variations in the modern and ancient earth and other planetary bodies, *in* Johnson, C.M., Beard, B.L., and Albarede, F., eds., Geochemistry of non-traditional stable isotopes: Reviews in Mineralogy and Geochemistry, v. 55, p. 319–357.

Beard, B.L., Johnson, C.M., Skulan, J.L., Nealson, K.H., Cox, L., and Sun, H., 2003, Application of Fe isotopes to tracing the geochemical and biological cycling of Fe: Chemical Geology, v. 195, p. 87–117.

Beaty, D.W., Taylor, H.P., Jr., and Coads, P.R., 1988, An oxygen isotope study of the Kidd Creek, Ontario, massive sulfide deposit—Evidence for a ^{18}O ore fluid: Economic Geology, v. 83, p. 1–17.

Booij, E., Bettison-Varga, L., Farthing, D., and Staudigel, H., 2000, Pb-isotope systematics of a fossil hydrothermal system from the Troodos ophiolite, Cyprus—Evidence for a polyphased alteration history: Geochimica et Cosmochimica Acta, v. 64, p. 3559–3569.

Brown, P.E., 1998, Fluid inclusion modeling for hydrothermal systems, *in* Richards, J.P., and Larson, P.B., eds., Techniques in hydrothermal ore deposit geology: Reviews in Economic Geology, v. 10, p. 151–171.

Deb, M., Tiwary, A., and Palmer, M.R., 1997, Tourmaline in Proterozoic massive sulfide deposits from Rajasthan, India: Mineralium Deposita, v. 32, p. 94–99.

Ehrlich, S., Butler, I., Halicz, L., Rickard, D., Oldroyd, A., and Mathhews, A., 2004, Experimental study of the copper isotope fractionation between aqueous Cu(II) and covellite, CuS: Chemical Geology, v. 209, p. 259–269.

Fehn, U., Doe, B.R., and Delevaux, M.H., 1983, The distribution of lead isotopes and the origin of Kuroko ore deposits in the Hokuroku District, Japan, *in* Ohmoto, H., and Skinner, B.J., eds., The Kuroko and related volcanogenic massive sulfide deposits: Economic Geology Monograph 5, p. 488–506.

Fouquet, Y., and Marcoux, E., 1995, Lead isotope systematics in Pacific hydrothermal sulfide deposits: Journal of Geophysical Research, v. 100, p. 6025–6040.

Galley, A.G., Hannington, M.D., and Jonasson, I.R., 2007, Volcanogenic massive sulphide deposits, *in* Goodfellow, W.D., ed., Mineral deposits of Canada—A synthesis of major deposit-types, district metallogeny, the evolution of geological provinces, and exploration methods: Geological Association of Canada, Mineral Deposits Division, Special Publication 5, p. 141–161.

Gokce, A., and Gulcan, B., 2004, Lead and sulfur isotope evidence for the origin of the Inler Yaylasi lead zinc deposit, northern Turkey: Journal of Asian Earth Sciences, v. 26, p. 91–97.

Goodfellow, W.D., and McCutcheon, S.R., 2003, Geologic and genetic attributes of volcanic sediment-hosted massive sulfide deposits of the Bathurst mining camp, New Brunswick—A synthesis, *in* Goodfellow, W.D., McCutcheon, S.R., and Peter, J.M., eds., Massive sulfide deposits of the Bathurst mining camp, New Brunswick, and northern Maine: Economic Geology Monograph 11, p. 245–301.

Goodwin, C.I., Robinson, M., and Juras, S.J., 1996, Galena lead isotopes, Buttle Lake mining camp, Vancouver Island, British Columbia, Canada: Economic Geology, v. 91, p. 549–562.

Graham, I.J., Reyes, A.G., Wright, I.C., Peckett, K.M., Smith, I.E.M., and Arculus, R.J., 2008, Structure and petrology of newly discovered volcanic centers in the northern Kermadec-southern Tofa arc, South Pacific Ocean: Journal of Geophysical Research, v. 113, B08S02, 24 p., doi:10.1029/2007JB005453.

Green, G.R., Ohmoto, H., Date, J., and Takahashi, T., 1983, Whole-rock oxygen isotope distribution in the Fukazawa-Kosaka area, Hokuroku district, Japan, and its potential application to mineral exploration, *in* Ohmoto, H., and Skinner, B.J., eds., The Kuroko and related volcanogenic massive sulfide deposits: Economic Geology Monograph 5, p. 395–411.

Green, G.R., and Taheri, J., 1992, Stable isotopes and geochemistry as exploration indicators: Geological Survey of Tasmania Bulletin 70, p. 84–91.

Gulson, B.L., 1986, Lead isotopes in mineral exploration: Amsterdam, Elsevier, 245 p.

Halbach, P., Hansmann, W., Koppel, V., and Pracejus, B., 1997, Whole-rock and sulfide lead-isotope data from the hydrothermal JADE field in the Okinawa back-arc trough: Mineralium Deposita, v. 32, p. 70–78.

Haymon, R.M., 1983, Growth history of hydrothermal black smoker chimneys: Nature, v. 301, p. 695–698.

Holk, G.J., Taylor, B.E., and Galley, A.G., 2008, Oxygen isotope mapping of the Archean Sturgeon Lake caldera complex and VMS-related hydrothermal system, northwestern Ontario, Canada: Mineralium Deposita, v. 43, p. 623–640.

Hou, Z., Zaw, K., Xiaoming, Q., Qingtong, Y., Jinjie, Y., Mingji, X., Deming, F., and Xiannke, Y., 2001, Origin of the Gacun volcanic-hosted massive sulfide deposit in Sichuan, China—Fluid inclusion and oxygen isotope evidence: Economic Geology, v. 96, p. 1491–1512.

Humphris, S.E., and Tivey, M.K., 2000, A synthesis of geological and geochemical investigations of the TAG hydrothermal field—Insights into fluid flow and mixing processes in a hydrothermal system, *in* Dilek, Y., Moorse, E., Elthon, D., and Nicholas, A., eds., Ophiolites and oceanic crust—New insights from field studies and the ocean drilling program: Geological Society of America Special Paper 349, p. 213–236.

Huston, D.L., 1999, Stable isotopes and their significance for understanding the genesis of volcanic-hosted massive sulfide deposits—A review, *in* Barrie, C.T., and Hannington, M.D., eds., Volcanic-associated massive sulfide deposits—Processes and examples in modern and ancient settings: Reviews in Economic Geology, v. 8, p.157–179.

Huston, D.L., and Taylor, B.E., 1999, Genetic significance of oxygen and hydrogen isotope variations at the Kidd Creek volcanic-hosted massive sulfide deposit, Ontario, Canada, *in* Hannington, M.D., and Barrie, C.T., eds., The giant Kidd Creek volcanogenic massive sulfide deposit, western Abitibi subprovince, Canada: Economic Geology Monograph 10, p. 335–350.

Inverno, C.M.C., Lopes, C.J.C.D., d'Orey, F.L.C., and de Carvalho, D., 2000, The Cu-(Au) stockwork of Salgadinho, Cercal, Pyrite Belt, SW Portugal—Paragenetic sequence and fluid inclusion investigations, *in* Gemmell, J.B., and Pongratz, J., eds., Volcanic environments and massive sulfide deposits: University of Tasmania, Australian Research Council, Center of Excellence in Ore Deposits (CODES) Special Publication 3, p. 99–101.

Ioannou, S.E., Spooner, E.T.C., and Barrie, C.T., 2007, Fluid temperature and salinity characteristics of the Matagami volcanogenic massive sulfide district, Quebec: Economic Geology, v. 102, p. 691–713.

James, R.H., Elderfield, H., and Palmer, M.R., 1995, The chemistry of hydrothermal fluids from the Broken Spur site, 29°N Mid-Atlantic Ridge: Geochimica et Cosmochimica Acta, v. 59, p. 651–659.

John, S.G., Rouxel, O.J., Craddock, P.R., Engwell, A.M., and Boyle, E.A., 2008, Zinc stable isotopes in seafloor hydrothermal vent fluids and chimneys: Earth and Planetary Science Letters, v. 269, p.17–28.

Johnson, C.M., Beard, B.L., Roden, E.E., Newman, D.K., and Nealson, K.H., 2004, Isotopic constraints on biogeochemical cycling of Fe, *in* Johnson, C.M., Beard, B.L., and Albarede, F., eds., Geochemistry of non-traditional stable isotopes: Reviews in Mineralogy and Geochemistry, v.55, p. 359–408.

Johnson, T.M., and Bullen, T.D., 2004, Mass-dependent fractionation of selenium and chromium isotopes in low-temperature environments, *in* Johnson, C.M., Beard, B.L., and Albarede, F., eds., Geochemistry of non-traditional stable isotopes: Reviews in Mineralogy and Geochemistry, v. 55, p. 289–317.

Larson, P.B., Maher, K., Ramos, F.C., Chang, Z., Gaspar, M., and Meinert, L.D., 2003, Copper isotope ratios in magmatic and hydrothermal ore forming environments: Chemical geology, v. 201, p. 337–350.

Marcoux, E., 1998, Lead isotope systematics of the giant massive sulfide deposits in the Iberian Pyrite Belt: Mineralium Deposita, v. 33, p. 45–58.

Maréchel, C.D., Télouk, P., and Albarède, F., 1999, Precise analysis of copper and zinc isotopic compositions by plasma-source mass spectrometry: Chemical Geology, v. 156, p. 251–273.

Marignac, C., Diagana, B., Cathelineau, M., Boiron, M-C., Banks, D., Fourcade, S., and Vallance, J., 2003, Remobilization of base metals and gold by Variscan metamorphic fluids in the southern Iberian pyrite belt—Evidence from the Tharsis deposit: Chemical Geology, v. 194, p. 143–165.

Markl, G., Lahaye, Y., and Schwinn, G., 2006, Copper isotopes as monitors of redox processes in hydrothermal mineralization: Geochimica et Cosmochimica Acta, v. 70, p. 4215–4228.

Marumo, K., Urabe, T., Goto, A., Takano, Y., and Nakaseama, M., 2008, Mineralogy and isotope geochemistry of active hydrothermal field at Suiyo seamount, Izu-Bonin arc, west Pacific Ocean: Resource Geology, v. 58, p. 220–248.

Mason, T.F.D., Weiss, D.J., Chapman, J.B., Wilkinson, J.J., Tessalina, S.G., Spiro, B., Horstwood, M.S.A., Spratt, J., and Coles, B.J., 2005, Zn and Cu isotopic variability in the Alexandrinka volcanic-hoted massive sulfide (VHMS) ore deposit, Urals, Russia: Chemical Geology, v. 221, p. 170–187.

Mathur, R., Ruiz, J., Titley, S., Liermann, L., Buss, H., and Brantley, S.L., 2005, Cu isotope fractionation in the supergene environment with and without bacteria: Geochemica et Cosmochimica Acta, v. 69, p. 5233–5246.

Mathur, R., Titley, S., Bara, F., Brantley, S., Wilson, M., Phillips, A., Munizaga, F., Maksaev, V., Vervoort, J., and Hart, G., 2009, Exploration potential of Cu isotope fractionation in porphyry copper deposits: Journal of Geochemical Exploration, v. 102, p. 1–6.

McCollom, T., and Shock, E.L., 1997, Geochemical constraints on chemolithoautotrophic metabolism by microorganisms in seafloor hydrothermal systems: Geochimica et Cosmochimica Acta, v. 61, p. 4375–4391.

Mortensen, J.K., Dusel-Bacon, C., Hunt, J., and Gabites, J., 2006, Lead isotopic constraints on the metallogeny of middle and late Paleozoic syngenetic base metal occurrences in the Yukon-Tanana and Slide Mountain/Seventymile Terranes and adjacent portions of the North American miogeocline, *in* Colpron, M., and Nelson, J.L., eds., Paleozoic evolution and metallogeny of pericratonic terranes at the ancient Pacific margin of North America, Canadian and Alaskan Cordillera: Geological Association of Canada, Special Paper 45, p. 261–279.

Mortensen, J.K., Hall, B.V., Bissig, T., Friedman, R.M., Danielson, T., Oliver, J., Rhys, D.A., Ross, K.V., and Gabites, J.E., 2008, Age and paleotectonic setting of volcanogenic massive sulfide deposits in the Guerrero Terrane of central Mexico—Constraints from U-Pb age and Pb isotope studies: Economic Geology, v. 103, p. 117–140.

Moura, A., 2005, Fluids from the Neves Corvo massive sulfide ores, Iberian Pyrite Belt, Portugal: Chemical Geology, v. 223, p. 153–169.

Nehlig, P., Cassard, D., and Marcoux, E., 1998, Geometry and genesis of feeder zones of massive sulfide deposits—Constraints from the Rio Tinto ore deposit (Spain): Mineralium Deposita, v. 33, p. 137–149.

Ohmoto, H., 1986, Stable isotope geochemistry of ore deposits: Reviews in Mineralogy, v. 16, p. 491–559.

Palmer, M., and Slack, J.F., 1989, Boron isotope composition of tourmaline from massive sulfide deposits and tourmalinites: Contributions to Mineralogy and Petrology, v. 103, p. 434–451.

Palmer, M.R., 1996, Hydration and uplift of the oceanic crust on the Mid-Atlantic Ridge associated with hydrothermal activity—Evidence from boron isotopes: Geophysical Research Letters, v. 23, p. 3479–3482.

Petersen, S., Herzig, P.M., and Hannnington, M.D., 2000, Third dimension of a presently forming VMS deposit—TAG hydrothermal mound, Mid-Atlantic Ridge, 26°N: Mineralium Deposita, v. 35, p. 233–259.

Pisutha-Arnond, V., and Ohmoto, H., 1983, Thermal history and chemical and isotopic compositions of the ore-forming fluids responsible for the Kuroko massive sulfide deposits in the Hokuroku District of Japan, *in* Ohmoto, H., and Skinner, B.J., eds., The Kuroko and related volcanogenic massive sulfide deposits: Economic Geology Monograph 5, p. 523–558.

Rouxel, O., Fouquet, Y., and Ludden, J.N., 2004a, Subsurface processes at the Lucky Strike hydrothermal field, Mid-Atlantic Ridge—Evidence from sulfur, selenium, and iron isotopes: Geochimica et Cosmochimica Acta, v. 68, p. 2295–2311.

Rouxel, O., Fouquet, Y., and Ludden, J.N., 2004b, Copper isotope systematics of the Lucky Strike, Rainbow, and Logachev sea-floor hydrothermal fields on the Mid-Atlantic Ridge: Economic Geology, v. 99, p. 585–600.

Rouxel, O., Ludden, J., Carignon, J., Marin, L., and Fouquet, Y., 2002, Natural variations of Se isotopic composition determined by hydride generation multiple collector coupled mass spectrometry: Geochimica et Cosmochimica Acta, v. 66, p. 3191–3193.

Rouxel, O., Shanks, W.C., Bach, W., and Edwards, K., 2008, Integrated Fe and S isotope study of seafloor hydrothermal vents at East Pacific Rise 9-10°N: Geochimica et Cosmochimica Acta, v. 252, p. 214–227.

Sanchez-Espana, J., Velasco, F., and Yusta, I., 2000, Hydrothermal alteration of felsic volcanic rocks associated with massive sulfide deposition in the northern Iberian Pyrite Belt (SW Spain): Applied Geochemistry, v. 15, p. 1265–1290.

Sangster, D.F., 1968, Relative sulphur isotope abundances of ancient seas and strata-bound sulfide deposits: Proceedings of the Geological Association of Canada, v. 19, p. 79–91.

Sangster, D.F., Outridge, P.M., and Davis, W.J., 2000, Stable lead isotope characteristics of lead ore deposits of environmental significance: Environmental Reviews, v. 8, p. 115–147.

Seyfried, W.E., Jr., and Shanks, W.C., III, 2004, Alteration and mass transport in mid-ocean ridge hydrothermal systems—Controls on the chemical and isotopic evolution of high-temperature crustal fluids, *in* Davis, E.E., and Elderfield, H., eds., Hydrogeology of the oceanic lithosphere: Cambridge, Cambridge University Press, p. 451–458.

Shanks, W.C., III, 2001, Stable isotopes in seafloor hydrothermal systems—Vent fluids, hydrothermal deposits, hydrothermal alteration, and microbial processes, *in* Valley, J.W., and Cole, D.R., eds., Stable isotope geochemistry: Reviews in Mineralogy and Geochemistry, v. 43, p. 469–525.

Shepherd, T.J., and Rankin, A.H., 1998, Fluid inclusion techniques of analysis, *in* Richards, J.P., and Larson, P.B., eds., Techniques in hydrothermal ore deposit geology: Reviews in Economic Geology, v.10, p. 125–149.

Sherlock, R.L., Roth, T., Spooner, E.T.C., and Bray, C.J., 1999, Origin of the Eskay Creek precious metal-rich volcanogenic massive sulfide deposit—Fluid inclusion and stable isotope evidence: Economic Geology, v. 94, p. 803–824.

Shwarz-Schampera, U., and Herzig, P.M., 2002, Indium geology, mineralogy and economics: Berlin, Springer, 257 p.

Sillitoe, R.H., Hannington, M.D., and Thompson, J.F.H., 1996, High sulfidation deposits in the volcanogenic massive sulfide environment: Economic Geology, v. 91, p. 204–212.

Slack, J.F., Ridley, W.I., Dusel-Bacon, C., and Fayek, M., 2008, Extreme sulfur isotope variation in the Dry Creek volcanogenic massive sulfide deposit, east-central Alaska: Geochimica et Cosmochimica Acta, v. 72, p. A876.

Spivack, A.J., Berndt, M.E., and Seyfried, W.E., 1990, Boron isotope fractionation during supercritical phase separation: Geochimica et Cosmochimica Acta, v. 54, p. 2337–2339.

Spivack, A.J., and Edmond, J.M., 1987, Boron isotope exchange between seawater and the oceanic crust: Geochimica et Cosmochimica Acta, v. 51, p. 1033–1043.

Stolz, J., and Large, R.R., 1992, Evaluation of the source-rock control on precious metal grades in volcanic-hosted massive sulfide deposits from western Tasmania: Economic Geology, v. 87, p. 720–738.

Taylor, B.E., and Huston, D.L., 1999, Regional ^{18}O zoning and hydrogen isotope studies in the Kidd Creek volcanic complex, Timmins, Ontario, *in* Hannington, M.D., and Barrie, C.T., eds., The giant Kidd Creek volcanogenic massive sulfide deposit, western Abitibi subprovince, Canada: Economic Geology Monograph 10, p. 351–378.

Taylor, H.P., 1977, Water/rock interactions and the origin of H_2O in granitic batholiths: Journal of the Geological Society of London, v. 133, p. 509–558.

Wilkinson, J.J., Weiss, D.J., Mason, T.F.D., and Coles, B.J., 2005, Zinc isotope variation in hydrothermal systems—Preliminary evidence from the Irish Midlands ore field: Economic Geology, v. 100, p. 583–590.

Zaw, K., Gemmell, J.B., Large, R.R., Mernagh, T.P., and Ryan, C.G., 1996, Evolution and source of ore fluids in the stringer system, Hellyer VHMS deposit, Tasmania, Australia—Evidence from fluid inclusion microthermometry and geochemistry: Ore Geology Reviews, v. 10, p. 251–278.

Zhu, X.K., O'Nions, R.K., Guo, Y., Belshaw, N.S., and Rickard, D., 2000, Determination of the natural Cu-isotope variation by plasma-source mass spectrometry—Implications for use as geochemical tracers: Chemical Geology, v. 163, p. 139–149.